JOURNAL OF SOLID STATE CHEMISTRY 119, 380–393 (1995)

Electronic Structure of Tetrahedral Iron(III)–Sulfur Clusters in Alkaline Thioferrates: An X-Ray Absorption Study

M. Atanasov[1]

Institute of General and Inorganic Chemistry, Bulgarian Academy of Sciences, Sofia 1113, Bulgaria

and

R. H. Potze and G. A. Sawatzky

Department of Applied and Solid State Physics, Materials Science Center, University of Groningen, Nijenborgh 4, 9747 AG Groningen, The Netherlands

Received March 29, 1995; accepted June 8, 1995

X-ray absorption spectra of Na_5FeS_4 and $KFeS_2$ containing separate and interconnected edge-shared FeS_4^{5-} tetrahedra, respectively, are reported and interpreted in terms of an $S = 5/2$ ground state for Fe^{3+} in both compounds. A rather small value of the ligand-to-metal charge transfer energy Δ_{eff} was indicated by the comparison of the experimental Fe $2p$ XAS spectrum with atomic multiplet calculations, reflecting an almost 1 : 1 admixture of d^5 and d^6L (L hole on the ligand) character in the ground state for Na_5FeS_4. The broadening of the main peak toward higher energies when going from Na_5FeS_4 to $KFeS_2$ is attributed to symmetry lowering from T_d to D_{2d}. Ligand-field parameterization schemes, such as the angular overlap model, are found to be quantitatively not applicable for the systems under consideration. The phase diagram of d^5 ions and its dependence on the crystal-field splitting (10Dq) and the ligand-to-metal charge transfer energy (Δ_{eff}) are discussed and it is shown that an intermediate spin state ($S = 3/2$) can become stable for negative Δ_{eff} and moderate values of 10Dq and metal–ligand hybridization. This presents another limit for the ligand-field approach and the Tanabe–Sugano diagrams, where only $S = 5/2$ and $S = 1/2$ ground states are predicted. For the Fe^{3+} in a tetrahedral field the theory indicates that it is unlikely that the $S = 3/2$ and $S = 1/2$ states become the ground state since the gain in energy due to ligand–ligand coupling and the relatively small charge transfer energy (both tending to lower energetically the $S = 3/2$ state) are not sufficient to overcome the high exchange stabilization of the high-spin ($S = 5/2$) state. © 1995 Academic Press, Inc.

I. INTRODUCTION

Alkaline iron(III) chalcogenides $A_xFe_yX_z$ (A = K, Rb, Cs; X = S, Se, Te) containing tetrahedral FeS_4^{5-} units have been the subject of a long-standing controversy regarding their electronic structure and ground state spin multiplicity. Varying the content (x) of the alkaline ion, it was possible to synthesize ionic lattices with separated FeS_4^{5-} tetrahedra (in Na_5FeS_4 (1)), dimeric units consisting of bitetrahedra sharing common edges ($Fe_2S_6^{6-}$ in Na_3FeS_3 (2)), and linear chains with $[FeS_2]^-$ units and FeS_4^{5-} tetrahedra slightly elongated along the pseudo-S_4-axis, extending in one dimension (in $AFeS_2$, A = K, Rb, Cs (3a, 3b)). In addition, $CsGaS_2$ with the same structures as $KFeS_2$ and $RbFeS_2$ was used as a host material in which Ga^{3+} was substituted with Fe^{3+} up to 25% without changing the crystal structure (4). Structural views for Na_5FeS_4 and $KFeS_2$, adopted from references (1) and (3b), respectively, are shown in Fig. 1.

Magnetic, optical, and neutron diffraction experiments, together with Mössbauer data on these systems, offer the unique possibility of following experimentally the cooperative effects that evolve in going from separate coordination units FeS_4^{5-}, to dimers, to one-dimensional chains. Fe(III) is a d^5 ion and according to ligand field theory, in a cubic field it can assume either a high-spin, $S = 5/2$, $e^2t_2^3$ configuration or a low-spin, $S = 1/2$, $e^4t_2^1$ configuration. In tetrahedral coordination with an $e < t_2$ splitting pattern and a 10Dq which is 4/9 from the octahedral value, it is expected that a high-spin ($S = 5/2$) state will be stabilized, although one should realize that the interatomic distances are smaller for the tetrahedral site, increasing the 10Dq value slightly. In line with this, magnetic measurements at temperatures higher than the Néel point (T_N = 28K) show

[1] To whom correspondence should be addressed at Institute für Theoretische Chemie, Heinrich-Heine Universität, Universitätsstrasse 1, Geb.26.32, D-40225 Düsseldorf, Germany.

0022-4596/95 $12.00

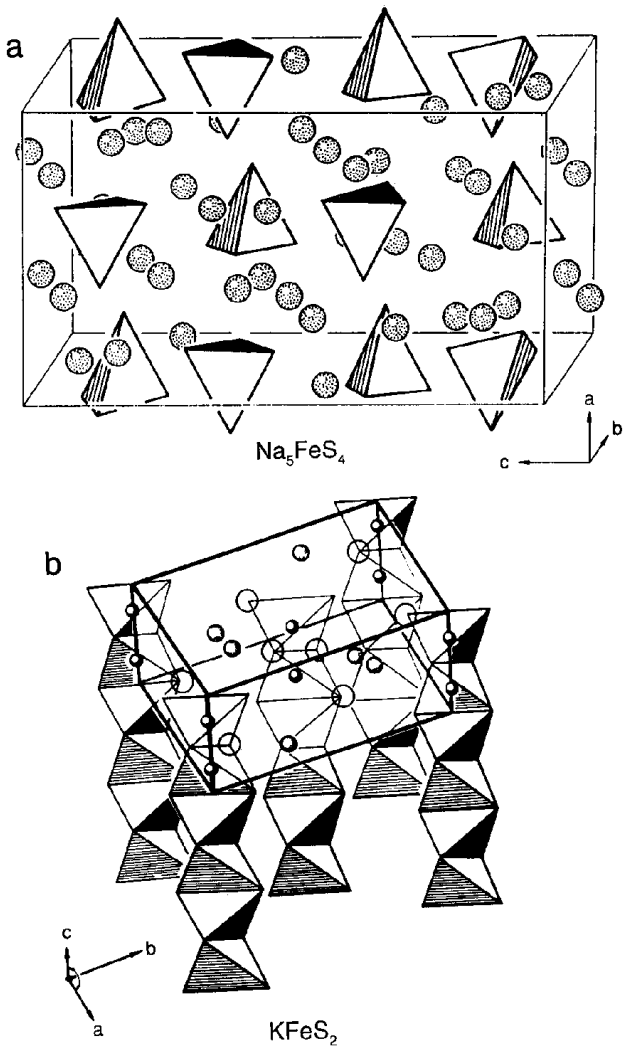

FIG. 1. Tetrahedral framework structures: (a) isolated tetrahedra in Na_5FeS_4 (adopted from Ref. (1)); (b) chains of edge-sharing tetrahedra in $KFeS_2$ (adopted from Ref. (3b)).

Curie–Weiss behavior for Na_5FeS_4 with an effective magnetic moment of 5.6 μ_B, indicating five unpaired electrons on iron ($S = 5/2$ spin only value, 5.96 μ_B) (1). The local magnetic moments appear to be strongly reduced, however, on going to dimers and chains, as shown by neutron diffraction data ($\mu = 2S\,\mu_B$: 1.9 μ_B, $KFeS_2$; 1.8 μ_B, $RbFeS_2$ (5)) and magnetic hyperfine fields from Mössbauer experiments (221 kG for $KFeS_2$ and 192 kG for $RbFeS_2$ (6a, 6b)), which are small compared to the mostly ionic Fe^{3+} oxides and fluorides (350–550 kG). A spin-pairing mechanism ($S = 1/2$) has been proposed, with the aim of explaining also the magnetic susceptibility data of $CsGa_{1-x}Fe_xS_2$ ($0 < x < 0.25$) in dependence on x (4). The Néel temperature of $KFeS_2$ ($T_N = 250$ K) reflects a three-dimensional magnetic ordering composed of a strong correlation between spins within the chain and a rather weak spin-coupling between chains. However, cooperative effects (antiferromagnetic coupling) strongly complicate such an $S = 1/2$ spin interpretation. Cooperative optical effects are also indicated by the polarized spectra on the $CsGa_{1-x}Fe_xS_2$ mixed crystals, as manifested by the strong dichroism in the visible region and the near-band edge intensity shape in polarization parallel to the chain, even at Fe^{3+} concentrations as low as 1% (7). The absorption spectra of the pure chain compounds are dominated by three broad maxima at 15,100, 18,800, and 23,000 cm^{-1} and have been ascribed to d–d transitions within the high-spin d^5 FeS_4^{5-} chromophore (8). A subsequent reinterpretation based on the high intensity, in terms of a ligand-to-metal charge transfer transition, has been proposed (7), while the weaker features between 8000 and 17,000 cm^{-1} in the Fe^{III}-doped $CsGeS_2$ have been attributed to purely d–d transitions within the d^5 states manifold.

In the studies so far, interpretations of magnetic and optic data on these compounds have been confined to ligand-field calculations within the d^5 configurations (7, 8, 15), or to extended Hückel or unrestricted Hartree–Fock calculations of the orbital levels (9, 10), disregarding the important role of correlation effects. Attempts to account for the latter have been made with variable success using the X_α-SW MO method (11, 12, 13a, 13b) and in the broken symmetry spin-polarized X_α-VB-SW calculations (12, 14). In ligand-field treatments, interactions of d^5 with the d^6L (L hole on the ligand) charge transfer states are accounted for in an effective way by an appropriate choice of the one-electron parameters of the ligand field from a fit to the experimental data. Thus it is tacitly assumed that d^5 and d^6L multiplets are energetically well separated, which certainly is not valid for the rather covalent Fe–S bond. Experimental data indicate, indeed, that the S^{2-} orbitals are rather close in energy to the 3d orbitals. Attempts to explain the reduced magnetic moments within the same approach have been given in terms of an $S = 1/2$ ground state of Fe^{3+} in the chains and even an intermediate $S = 3/2$ local spin state for the dimers (16).

In this paper $2p^63d^5 \rightarrow 2p^53d^6$ high-resolution X-ray absorption spectra on $KFeS_2$ containing FeS_2 chains are reported and compared with the spectra of Na_5FeS_4 containing separate FeS_4^{5-} ($S = 5/2$) units. We show that the local spin states in both compounds are the same ($S = 5/2$), excluding the $S = 1/2$ and $S = 3/2$ states as possible alternatives. An interpretation of the spectral band shapes in terms of a model Hamiltonian which takes explicit account of the d^6L and d^7L^2 charge transfer states provides an indication for the model parameters from a fit to the observed band profiles. The model parameters are compared with Harrison-like (17) calculations of the orbital levels for Fe^{3+}, which interact with the MO orbitals of representative S_4^{8-} and S_8^{16-} clusters. A discussion of the changes in the absorption profiles on going from Na_5FeS_4

to $KFeS_2$ will be given. Using calculations within the d^5–d^6L–d^7L^2 configuration–interaction cluster model, a reinterpretation of the optical results is proposed as well. Finally, we will study in more detail the possible ground state spin multiplicities for d^5 ions in a tetrahedral field and the dependence on the parameters of the cluster CI model. Parameter ranges for high (S = 5/2), low (S = 1/2), and even intermediate (S = 3/2) spin states will be specified. In view of the possibility for ground states with a spin S = 3/2 in cases of negative to small ligand-to-metal charge transfer energies, limits for the application of the well-known Tanabe–Sugano diagrams are discussed.

II. EXPERIMENTAL

The X-ray absorption spectra (XAS) at the Fe2p edge were taken at the undulator 5U.1 at the SRS Daresbury. A number of crystals of both Na_5FeS_4 and $KFeS_2$ were measured in order to ensure consistency and reproducibility. All spectra were collected in a vacuum range of 10^{-7}–10^{-8} Torr. The spectra were taken in total electron yield mode, using a channeltron. The resolution at the Fe2p edge was about 450 meV.

In order to analyze the experimental data, a large number of multiplet energy and X-ray absorption intensity calculations were performed, using the chain groups approach given by Butler (18). This approach starts with the calculations of the reduced matrix elements of all necessary operators in the spherical group, realized using Cowan's atomic multiplet program (19a, 19b). The Wigner–Eckart theorem is then applied to obtain the reduced matrix elements in any desired point group. Butler's point-group program calculates the necessary isoscalar factors, using modern group theoretical results to obtain a consistent set of coefficients. Using this approach, a general program was developed by Thole (20a; see 20b–20d) with the advantage over standard methods of treating all point groups in a uniform way. The program can calculate transition energies and rates between any two configurations in X-ray absorption, photoemission, or inverse photoemission spectroscopy. The parameters used in these calculations, the d–d Coulomb repulsion energy U, the core-hole–d-electron Coulomb interaction Q, the ligand-to-metal charge transfer energy Δ, the metal–ligand overlap energies T_c and T_t, and the crystal field 10Dq, are treated as adjustable parameters. The d–d Coulomb repulsion energy (U) is defined by

$$U = E(d^6) + E(d^4) - 2E(d^5), \qquad [1]$$

where $E(3d^6)$, $E(3d^4)$, and $E(3d^5)$ denote the configuration-averaged energies of the $3d^6$, $3d^4$, and the $3d^5$ multiplets, respectively. In addition, the charge transfer energy Δ is by definition $E(3d^{n+1}L)$–$E(3d^n)$, where $E(3d^{n+1}L)$ and $E(3d^n)$ denote the configuration-averaged energies of the $3d^{n+1}L$ and $3d^n$ multiplets, respectively. The parameter Δ_{eff} for Fe^{3+} (d^5) is defined with respect to the respective ground states of the d^5 and d^6L multiplets:

$$\Delta_{eff} = \Delta + (28/9)J. \qquad [2]$$

The parameter U_{eff}, which for the $Fe^{3+}(d^5)$ is defined with respect to the respective $3d^6$, $3d^4$, and $3d^5$ ground states is related to U as

$$U_{eff} = U + (56/9)J, \qquad [3]$$

where

$$J = 3B + C \qquad [4]$$

is taken as the average from the intra-atomic (Hund) exchange integrals between e electrons ($4B + C$), t_2 electrons ($3B + C$), and between e and t_2 electrons ($2B + C$). The values of the Racah parameters B and C (and the related $F^2(d, d)$, $F^4(d, d)$ parameters) were reduced to 80% of their atomic Hartree–Fock values to account for intra-atomic relaxation effects (19b). A list of ab initio Hartree–Fock values for the initial and final state configurations, including Fe 2p–3d Coulomb [$F^2(p, d)$, $G^1(p, d)$ and $G^3(p, d)$] and spin–orbit coupling parameters $\zeta(3d)$ and $\zeta(2p)$, is given in Table 1.

III. RESULTS AND DISCUSSION

III.1. $L_{2,3}$—X-Ray Absorption Spectra and the Spin State of Fe^{III} in Na_5FeS_4 and $KFeS_2$

The experimental $2p \rightarrow 3d$ XAS spectra of Na_5FeS_4 and $KFeS_2$ are depicted in Fig. 2. They consist of $2p_{3/2}(L_3)$ and $2p_{1/2}(L_2)$ branches with an energy separation of $1.5\zeta_p$, where ζ_p is the spin–orbit coupling constant. Comparing the spectra of Na_5FeS_4 with isolated FeS_4^{5-} units (S = 5/2 ground state) with the spectrum of $KFeS_2$ with interconnected FeS_4^{5-} polyhedra, one can state that (aside from some changes which will be discussed subsequently) the spectra are very similar. Comparing the details of the multiplet structure of experimental X-ray absorption spectra with atomic multiplet calculations provides a powerful tool for determining the local spin state of 3d transition metal ions in their compounds. The multiplet structure arises from the transitions $2p^63d^n \rightarrow 2p^53d^{n+1}$, where dipole selection rules strongly confine the subset of final states that can be reached from the ground state. In the low-spin ground state, electrons pair up in orbitals with the lowest energy, while in the high-spin ground state higher orbitals are also occupied with the spins parallel. In the five-particle

TABLE 1
Ab initio Hartree–Fock Values of the Parameters (eV) of the Initial and Final State Configurations

	$F^2(d,d)$ (B)	$F^4(d,d)$ (C)	J	$\zeta(3d)$	$F^2(p,d)$	$G^1(p,d)$	$G^3(p,d)$	$\zeta(2p)$
$Fe^{3+}2p^63d^5$	12.043	7.535	1.079	0.059	—	—	—	—
	(0.160)	(0.598)						
$Fe^{2+}2p^63d^6$	10.966	6.815	0.980	0.052	—	—	—	—
	(0.146)	(0.541)						
$Fe^{1+}2p^63d^7$	9.762	6.018	0.870	0.046	—	—	—	—
	(0.131)	(0.478)						
$Fe^{3+}2p^53d^6$	12.818	8.023	1.149	0.074	7.446	5.566	3.166	8.199
	(0.171)	(0.637)						
$Fe^{2+}2p^53d^7$	11.779	7.327	1.053	0.067	6.793	5.004	2.844	8.200
	(0.157)	(0.582)						
$Fe^{1+}2p^53d^8$	10.623	6.560	0.948	0.059	6.143	4.467	2.538	8.202
	(0.142)	(0.521)						

Note. The actual values for the Coulomb and exchange interactions have been scaled to 80% of these values. Spin–orbit coupling parameters $\zeta(3d)$ and $\zeta(2p)$ are taken without reduction.

case of $Fe^{3+}(d^5)$ this results in distinctly different types of XAS spectra, which can be used as a fingerprint for high spin or low spin. Crystal-field interaction mixes states with different L in the ground LS-term, allowing transitions to other final states with the same spin. This gives rise to a broadening of the peaks and a gradual appearance of new peaks with increasing crystal field strength (10Dq). XAS profiles for $Fe(d^5)$ in T_d coordination and variable cubic splitting, 10Dq values are depicted in Fig. 3 (adopted from Ref. (20c)). In these calculations hybridization[2] was not taken into account. With increasing 10Dq a change from $S = 5/2$ to $S = 1/2$ takes place when the 10Dq parameter becomes larger than the $5/2 \rightarrow 1/2$ spin-pairing energy. In the same direction the weaker transition at the higher energy side of the L_3 branch disappears, while an additional transition at the lower energy side of the L_3 branch grows in intensity. Comparison of Fig. 3 with the experimental spectrum in Fig. 2 lends further support to the idea that both compounds Na_5FeS_4 and $KFeS_2$ are characterized by similar parameter values appropriate for a high-spin $S = 5/2$ ground state.

III.2. XAS and Covalency Effects in FeS_4 Clusters: A Charge Transfer Model for the Fe–S Bonding

III.2.1. The spectrum of Na_5FeS_4. In the previous section only crystal-field effects have been taken into account. The cubic symmetry is accounted for in terms of a single parameter, 10Dq, the role of which is just to split the d orbitals in cubic symmetry into two- $e(x^2\text{-}y^2, 3z^2\text{-}r^2)$ and threefold $t_2(xy, xz, \text{and } yz)$ degenerate sublevels. In the following, covalency effects due to hybridization of the d^5 with the d^6L and d^7L charge transfer states, which were neglected in previous studies, will be explicitly considered. A schematic presentation of the coupling of electronic configurations in the initial and final states with appropriate parameters is illustrated in Fig. 4.

Diagonal matrix elements are parametrized in terms of the parameters of $3d$–$3d$ and $2p$–$3d$ Coulomb interactions U and Q, respectively (see Section II).

The initial and final states originating from the ionic Fe^{3+} $2p^63d^5$ and $2p^53d^6$ states couple with the multiplets of the same symmetry which result from transferring a single electron from the $3p$ orbitals of S to Fe ($2p^63d^6L$ and $2p^5d^7L$, respectively). The nearest neighbor ligand-to-metal $2p$–$3d$ hopping elements, which couple the ionic

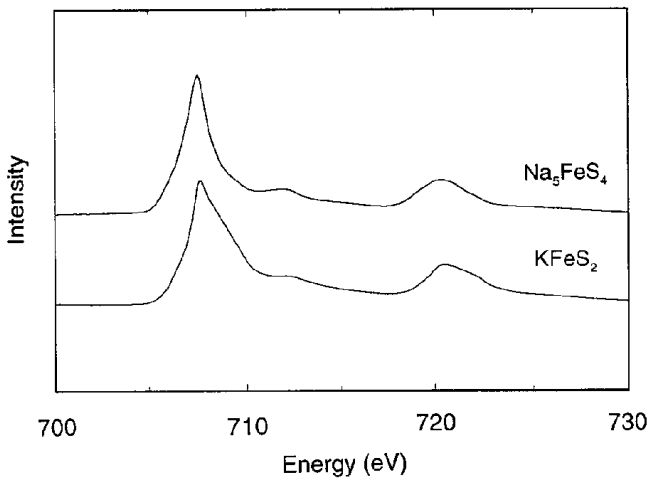

FIG. 2. Experimental Fe2p XAS data on Na_5FeS_4 (isolated FeS_4 tetrahedra) and $KFeS_2$ (edge-sharing FeS_4 tetrahedra).

[2] Hybridization, used in a different sense than in chemistry, means the interaction of orbitals of different centers via the effective one-electron Hamiltonian.

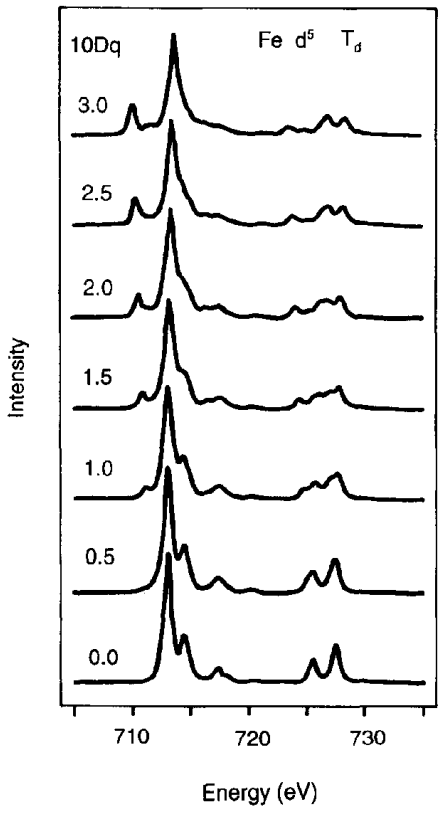

FIG. 3. Calculated $2p$ absorption spectra for $Fe^{3+}(d^5)$ in tetrahedral (T_d) geometry (adopted from Ref. (20c)). The Slater integrals and spin–orbit parameters are 80 and 100% of the free ionic values, respectively.

d^5 states with the d^6L and the d^6L with the d^7L^2 charge transfer states, are expressed in terms of Slater–Coster integrals $(pd\sigma)$ and $(pd\pi)$ (21). T_t and T_e integrals are introduced to represent hybridization between the $3d$ orbitals of t_2 and e symmetry, respectively, and the corresponding ligand orbitals of the same symmetry.

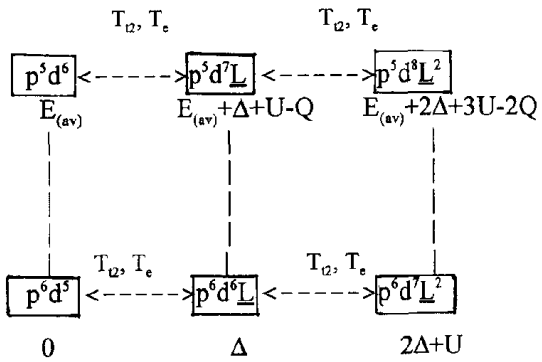

FIG. 4. A parametric scheme for the XAS initial and final states and their energies for d^5 ions including hybridization with singly and doubly excited ligand-to-metal charge transfer configurations. For a definition of the model parameters, see text.

The contributions to T_t and T_e are easily calculated using the one-electron secular matrices:

$$\begin{array}{c} \begin{matrix} t_2[d^5] & t_2[d^6L(\sigma)] & t_2[d^6L(\pi)] \end{matrix} \\ \begin{pmatrix} 0 & [(2/\sqrt{3})(pd\sigma)] & [(2\sqrt{2}/3)(pd\pi)] \\ [(2/\sqrt{3})(pd\sigma)] & \delta & 0 \\ [(2\sqrt{2}/3)(pd\pi)] & 0 & \delta \end{pmatrix} \end{array} \quad [5]$$

$$\begin{array}{c} \begin{matrix} e(d^5) & e[d^6L(\pi)] \end{matrix} \\ \begin{pmatrix} 0 & [2\sqrt{(2/3)}(pd\pi)] \\ [2\sqrt{(2/3)}(pd\pi)] & \delta \end{pmatrix}. \end{array} \quad [6]$$

In these equations we used δ as a notation of the orbital transfer energy as defined by the energy separation between the baricenters of the e, t_2 orbitals of the metal and the ligands. The following relationship between the parameters δ and Δ_{eff} can be derived if one takes the ${}^6A_1(d^5)$ and ${}^6A_1[d^6t_2(L)]$ terms as energy references for d^5 and d^6L, respectively:

$$\Delta_{\text{eff}} = \delta + 4\text{Dq} + 5U. \quad [7]$$

Note that the coupling between the e orbitals is represented by a single parameter $T_e = [2\sqrt{(2/3)}(pd\pi)]$ (Eq. [6]), reflecting the covalent mixing between the d^5 and the d^6L multiplets, for orbitals of e type, while two independent parameters, $T_t(\sigma) = [(2/\sqrt{3})(pd\sigma)]$ and $T_t(\pi) = [(2\sqrt{2}/3)(pd\pi)]$, are needed for orbitals of t_2 type (Eq. [5]). This results in a markedly different bonding scheme as compared to octahedral complexes, where ligand orbitals contribute by unique combinations of $e_g(\sigma)$ and $t_{2g}(\pi)$ symmetries.

In Eqs. [5] and [6] ligand–ligand hybridization is not taken into account. In order to study the effect of the latter as well as to obtain greater insight into the effects of covalency influencing the parameter values T_e and T_t we performed calculations on the FeS_4^{5-} clusters, using the method of Harrison (17) to estimate the matrix elements of metal–ligand, $V_{\text{ld}m}$, and ligand–ligand, $V_{\text{ll}'m}$ ($m = \sigma, \pi$), covalent mixing. The problem is divided into two steps. In the first step the orbitals Ψ_i^L and energies E_i^L of a S_4^{8-} tetrahedral cluster are obtained, considering ligand–ligand orbital coupling matrix elements only. In a second step, the coupling of the $3d$ orbitals with the resulting S_4^{8-} cluster orbitals Ψ_i^L are evaluated, yielding matrix elements for the t_2 and e symmetry species. The energies of the Fe^{3+}, $3d$ and S^{2-}, $3p$, $3s$ orbitals have been taken as -12.70, -13.30, and -20.00 eV, respectively (9). The resulting secular equations for the e- and t_2 symmetries are listed in Table

TABLE 2

S_4^{8-} Cluster Orbital Energies and Matrix Elements (in eV) of [Fe^{3+}, 3*d*]–[S_4^{8-}(3*s*,3*p*-*MO*)] Hybridization as Obtained from Harrison-type *MO*-LCAO Calculations[a]

$Fe^{3+}3d$ symmetry (T_d)	Cluster *MO* i =	1	2	3
e	E_i	−13.569		
	$(x^2 - y^2\|H\|\Psi_i)$	0.728		
	$(3z^2 - r^2\|H\|\Psi_i)$			
t_2	E_i	−13.797	−12.256	−19.526
	$(xy\|H\|\Psi_i)$			
	$(xz\|H\|\Psi_i)$	−0.121	1.410	−0.774
	$(yz\|H\|\Psi_i)$			

[a] Orbital energies adopted from Ref. (9) are $E(3p,S^{2-}) = -20.00$ eV, $E(3s,S^{2-}) = -13.3$ eV $E(3d, Fe^{3+}) = -12.7$ eV.

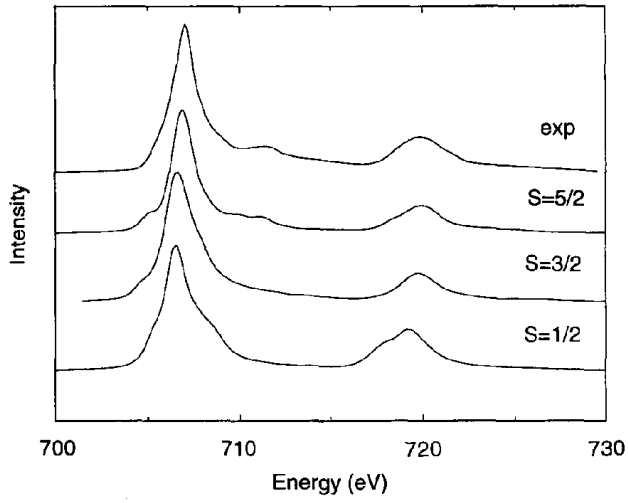

FIG. 5. Experimental and theoretical XAS spectra for Na_5FeS_4. Calculations for the high- (S = 5/2), intermediate- (S = 3/2), and low-spin (S = 1/2) initial states have been done with parameter values, listed in Table 2.

2. The t_2 coupling matrix can be reduced in a rather good approximation to a (2 × 2) problem, involving the 3*d* and $\Psi_2(L, 3p)$ basis functions only. The contributions from the functions $\Psi_1(L, 3p)$ and $\Psi_3(L, 3s)$ can be neglected; the first is essentially nonbonding, as is seen by the small 3*d*–3*p* off-diagonal element, the second (3*s* type) is fairly well separated in energy from 3*d*, yielding negligible coupling. It follows from these considerations that the basis set of the t_2 orbitals can be reduced in a rather good approximation to two basis functions of ligand and metal type, which mix by covalency via a single (effective) quantity denoted hereafter by T_t. The calculated value of T_t (1.410 eV) is found to be twice as large as the hopping integral of e type (T_e = 0.728 eV) (compare to the octahedral case where a T_e/T_t ratio of 2 has been proposed (22)). The splitting of the ligand orbitals t_2 and e we define as $\delta W = E[t_2(L)] - E[e(L)]$ is calculated to be 1.3 eV.[3]

The results from the cluster calculations have been used to reduce the number of model parameters as follows: the splitting of the ligand levels δW and the T_e/T_t parameter ratio were fixed at 1.3 eV and 0.5, respectively. Values of U and Q of 6 and 5 eV were adopted from data on related systems and a Q/U value of 0.83 (23a, 23b). The parameters T_t, Δ, and 10Dq were treated as adjustable parameters. The experimental spectrum together with the calculated spectra for high-, intermediate-, and low-spin ground states are shown in Fig. 5, while the parameters used in these calculations are listed in Table 3.

The calculated band shape was found to be most sensitive with respect to 10Dq and T_t and to a lesser extent to the parameters Δ, U, Q, and δW. The feature at the high-energy side seen in the experimental L_3 edge of Na_5FeS_4 (Fig. 2) could be only reproduced for values of 10Dq with a high-spin ground state on Fe^{3+}. The negative value of Δ shows that the center of gravity of the d^6L charge transfer states is at lower energy than the d^5 states (but note the still positive value for Δ_{eff} (Eq. [2], Δ_{eff} = 0.68 eV). However, there is a strong mixing between the two configurations as well as a small yet nonnegligible d^7L^2 contribution in the ground state:

$$\Psi_{g.st.} = \sqrt{(0.41)}|d^5\rangle + \sqrt{(0.52)}|d^6L\rangle + \sqrt{(0.07)}|d^7L^2\rangle. \quad [8]$$

The parameters Δ and T_t (Table 3) are comparable in sign and magnitude to those obtained from a recent study of the valence band photoemission spectra of the chalcopyrite-type $CuFeS_2$ compound (Δ = −0.5 eV, U = 4 eV) (24) but are markedly different compared to the parameter range for Δ (1.9—5.0 eV), deduced from core-level XPS spectra of $KFeS_2$ reported by Butcher *et al.* (25). One possible reason for this disagreement is the covalent mixing

TABLE 3

Summary of the Parameters (in eV) Used in the Calculation of the $L_{2,3}$-Edge XAS of Na_5FeS_4 for High- (S = 5/2), Intermediate- (S = 3/2), and Low-Spin (S = 1/2) Initial States

S	Δ	T_t	T_e	10Dq
5/2	−2.0	1.4	0.7	0.5
3/2	−5.0	1.4	0.7	0.78
1/2	−2.0	1.4	0.7	2.0

Note. In all three calculations U, Q, and δW have been taken to be 5.0, 6.0, and 1.3 eV, respectively (see text).

[3] With nonzero values of δW Eq. [7] must be modified as $\Delta_{eff} = \delta + 4Dq - (2/5)\,\delta W + 5U$.

matrix element $T = \langle d|H|L\rangle$, which was approximated in (25) as being the same for the e and the t_2 orbitals.

III.2.2. The spectrum of $KFeS_2$. As seen from Fig. 2, the $L_{2,3}$ edges of Na_5FeS_4 and $KFeS_2$ show a striking similarity with respect to their band shapes and maxima positions. However, there is a clear broadening of the main peak toward the high-energy side when going from Na_5FeS_4 to $KFeS_2$ (Fig. 2). Using the configuration interaction–charge transfer model described in Section III.2.1, we tried to reproduce the band shape by varying the model parameters 10Dq, T_t, and Δ. We were not able to reproduce the intensity distribution while maintaining the spectral features of the experimental spectrum. Starting with the parameters used in the Na_5FeS_4 calculation (Table 3, high-spin values), small changes in 10Dq, Δ, and T_t have little effect on the width of the main peak. Large variations alter the spectrum to a large extent when the spin of the ground state is changed. In particular, the shoulder at the high-energy side of the L_3 edge is not compatible with $S = 1/2$ and $S = 3/2$ ground states. In view of this, it is still the high-spin state which reproduces the overall spectral features of $KFeS_2$. However, the broadening indicates that upon going from separate to interconnected FeS_4^{5-} tetrahedra, the electronic levels of the high-spin Fe^{3+} are modified considerably by the presence of neighboring FeS_4^{5-} centers. Although superexchange has been recently shown to influence the XAS spectral shapes (26, 27a, 27b), the size of the effect is too small to explain the observed broadening.

Another contribution affecting the multiplet energies of Fe^{3+} originates from low symmetric fields due to ligand–ligand interactions as well as the perturbing effect of neighboring Fe^{3+} ions. The latter influences are electrostatic in origin and were explicitly accounted for by Bronger and Müller (15), who calculated the crystal field effect on a given Fe^{3+} induced by the S^{2-} in Fe^{3+} in the particular lattice sites. However, as follows from our consideration, the electrostatic charges of Fe^{3+} and S^{2-} should be strongly reduced by the rather covalent Fe–S interactions, leading to a rather small effect of Fe^{3+} on neighboring Fe^{3+} centers. In support of this, spin-polarized Slater Xα calculations give net charges on Fe^{3+} (+1.2) distinctly smaller than those assumed in the electrostatic calculation (15).

The second aspect concerns the bonding properties of S^{2-}, which may considerably change going from separate to interconnected FeS_4^{5-} units. As was shown by Silvestre and Hoffman (9), the orbitals of S^{2-} in the separate FeS_4^{5-} tetrahedra are optimally aligned for interactions between Fe^{3+} and S^{2-}. In a chain composed of FeS_4^{5-} tetrahedra connected via common edges, the orbitals of S^{2-} are shared between two tetrahedra and as such cannot be optimally aligned with respect to the metal–ligand and the ligand–ligand interactions at the same time. Thus, orbitals which contribute to σ bonding with iron (t_2) will be involved in weaker π interactions with neighboring sulfur atoms so that they will be insensitive with respect to increasing the cluster size. In contrast, going to the chain the only weakly π-interacting e orbitals of S acquire some σ-bonding components as well, inducing a stronger energy effect on the corresponding orbitals on the metal. The result of all these influences is a low symmetric field seen by each Fe^{3+} center even though the S^{2-} ions taken as point charges form regular tetrahedra around Fe^{3+}.

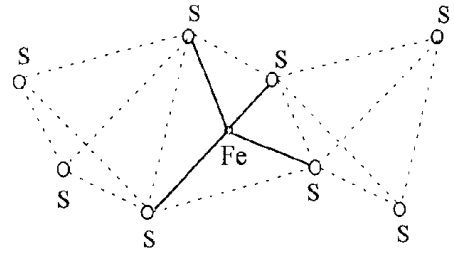

FIG. 6. The S_8^{16-} cluster hybridizing the $3d$ orbitals of Fe^{3+} placed at the position of the central S_4^{8-} tetrahedron. The site symmetry around Fe^{3+} is D_{2d}, the geometry of the nearest S_4^{8-} surrounding of Fe^{3+}, is regular tetrahedral.

We modeled the effect of ligand–ligand coupling by calculating the orbital levels of a S_8^{16-} cluster consisting of three S_4^{8-} moieties with a regular tetrahedral geometry (Fig. 6). Orbital matrix elements between ligands $3p$ and $3s$ basis functions were approximated, using formulas by Harrison (17) (see above). The resulting eigenfunctions were coupled with the $3d$ orbitals of Fe^{3-} placed at the central tetrahedral unit. The matrix elements between the various $3d$ orbitals of iron and their counterparts of appropriate symmetry from the S_8^{16-} cluster orbital levels are included in Table 4. The resulting secular equations, each including a single d orbital were diagonalized. The energy levels for the eigenfunctions of the FeS_8^{13-} with main participation from the $3d$ orbitals of Fe are depicted in Fig. 7 (dashed lines) and can be compared with the corresponding orbitals of a single FeS_4^{5-} moiety (solid lines). d Orbital percentages are also indicated.

There is a considerable splitting of the $3d$ orbitals of Fe^{3+}, reflecting the symmetry lowering from T_d to D_{2d} around iron in the FeS_8^{13-} cluster, compared with the separate FeS_4^{5-} units. Note that the S_4^{8-} point geometries in both calculations were taken as regular tetrahedra. As seen in Fig. 7, the energy changes are particularly pronounced for the z^2-type orbital, which also undergoes the most reduction in its $3d$ character (about twice that in FeS_4^{5-}). The reduction in the d-orbital percentage follows the energy shifts, as expected. The incorporation of the Fe^{3+} ions into the extended S_8^{16-} compared to the smaller S_4^{8-} cluster also leads to a shift in z^2 to an approximately 0.5-eV higher energy. The lowering of symmetry could explain the broadening of the $2p \rightarrow 3d$ absorption profile toward the high-energy side going from Na_5FeS_4 to $KFeS_2$. Also in strong

TABLE 4

S_8^{16-} Cluster Orbital Energies and Matrix Elements (in eV) of [Fe^{3+}, 3*d*]–[S_4^{8-} (3*s*,3*p*-*MO*)] Hybridization as Obtained from Harrison-type *MO*-LCAO Calculations[a]

$Fe^{3+}3d$ cluster *MO* (symmetry D_{2d})	i =	1	2	3	4	5	6	7	8
b_1	E_i	−13.792	−12.919						
	$(x^2 - y^2\|H\|\Psi_i)$	0.609	0.400						
a_1	E_i	−21.910	−19.973	−14.261	−14.073	−13.675	−12.214		
	$(3z^2 - r^2\|H\|\Psi_i)$	0.019	−0.066	−0.308	−0.336	0.191	−0.543		
b_2	E_i	−21.125	−18.836	−14.155	−13.730	−12.626	−12.063		
	$(xy\|H\|\Psi_i)$	−0.373	0.681	0.029	−0.109	−0.866	1.112		
e	E_i	−19.596	−19.486	−14.090	−13.575	−12.942	−12.513	−12.275	−12.001
	$(xy,yz\|H\|\Psi_i)$	−0.600	0.484	−0.066	0.090	0.473	−0.463	−0.678	1.050

[a] Orbital energies adopted from ref. (9) are $E(3p,S^{2-}) = -20.0$ eV; $E(3s,S^{2-}) = -13.3$ eV; $E(3d,Fe^{3+}) = -12.7$ eV.

support of the low-symmetric field around Fe^{3+} in the extended S_4^{8-} tetrahedral arrays is the polarization seen in the optical spectra (7) and the electric field gradients from Mössbauer data (6). The quadrupolar splittings manifested by the Mössbauer experiments range between 0.51 ($KFeS_2$) and 0.44 mm · s^{-1} ($CsFeS_2$) and can be attributed to overlap distortions of the 3*p* levels of Fe imposed by the surrounding ligands (28). As follows from the expressions of the z components of the electric field gradient (q'_{ov}) due to overlap contributions (28)

$$q'_{ov} = (4/5)e\langle r^{-3}\rangle_{3p}[2N_z^2 - N_x^2 - N_y^2]; \qquad [8]$$

the orbital contributions from $3p_z$, (N_z) and $3p_x$, $3p_y$(N_x, N_y) become essentially different in the lowered (D_{2d}) sym-

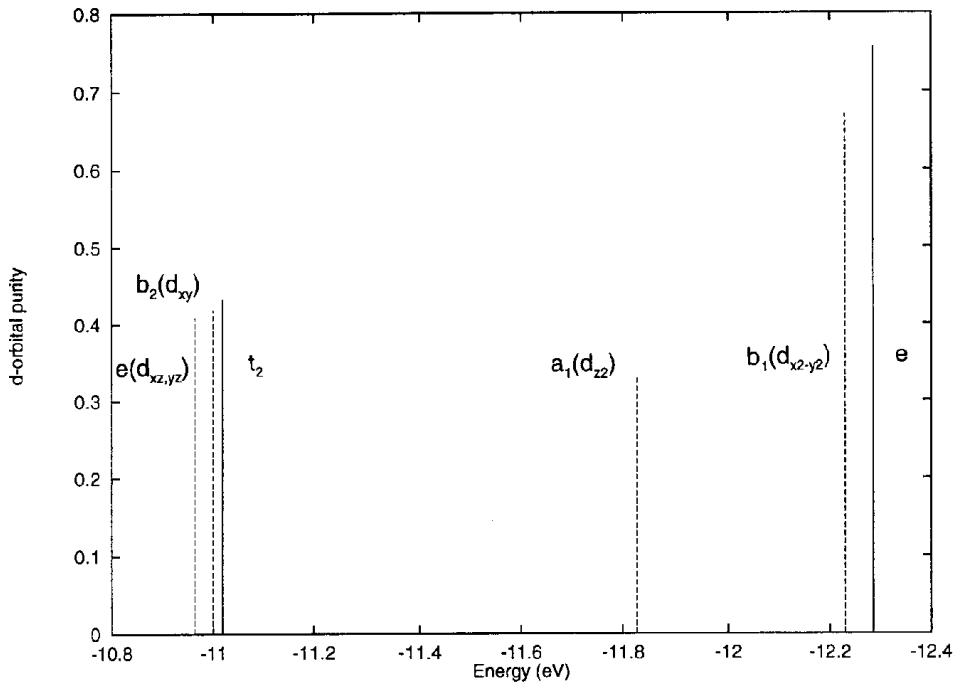

FIG. 7. *d* Orbital level scheme for an isolated FeS_4^{5-} tetrahedron (T_d symmetry, solid lines) and Fe^{3+} in S_8^{16-} (Fig. 6, D_{2d} symmetry, dashed lines). Orbital energies have been calculated using metal–ligand and ligand–ligand orbital matrix elements given by Harrison (Ref. (17)). Diagonal energies for the Fe^{3+} 3*d* and S^{2-} 3*s*, 3*p* orbitals have been adopted from Ref. (9). Note the splitting of the 3*d* orbitals of Fe^{3+} in the regular FeS_4 units due to the lowered symmetry due to ligand–ligand coupling.

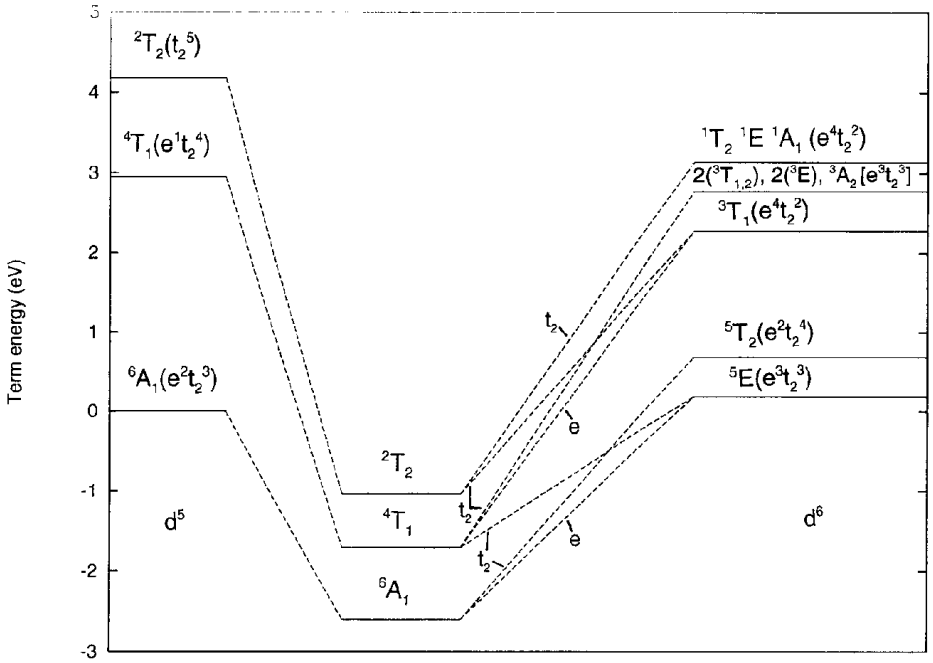

FIG. 8. The lowest ionic multiplets for d^5 (left) and d^6L (right) and the resulting term energy diagram after accounting for their hybridization (middle). The d^7L^2 states are not shown but have been taken into account in the calculations. For model parameters see Table 3 (high-spin ground state).

metry around Fe^{3+} in $KFeS_2$, No such contributions are expected for the only slightly distorted FeS_4 tetrahedra in Na_5FeS_4. Unfortunately, Mössbauer data on this compound are lacking.

III.4. d Electronic Levels and the Spin-Forbidden Transitions in FeS_4^{5-}

Term energies have been calculated for the d^5 configuration using parameters for the best fit [Table 2, high-spin (S = 5/2) values]. Mixing with the d^6L and d^7L^2 charge transfer states has been explicitly taken into account. A schematic term energy diagram, including the ground and the lowest excited states of d^5 and d^6L before and after accounting for their hybridization, is presented in Fig. 8. States due to d^7L^2 electronic configuration are not shown but have been taken into account in the numerical calculations. A list of theoretical values for the lowest transition energies as well the d^5 percentages for the ground $^6A_1$ and the first excited states $^4T_1$, $^4T_2$, and $^2T_2$ is given in Table 5. The calculated $^6A_1 \rightarrow {}^4T_1, {}^4T_2$, and $^2T_2$ transition energies (7180, 8630, and 12558 cm^{-1}) are in reasonable agreement with the experimental data reported by Solomon *et al.* for $Fe(SR)_4^-$ (R = 2,3,5,6-Mc_4C_6H, 7250, 7975, 9540, 10525, and 11235 cm^{-1}) (29), which show in addition low symmetric splitting of the tetrahedral parent $^4T_1$ and $^4T_2$ terms. Low-temperature absorption spectra in the near-IR and visible region on Na_5FeS_4 and $CsGa_{1-x}Fe_xS_2$ ($0.0 < x < 0.25$) have been reported as well (7). However, the spectra on the former compound were not very informative with regard to the spin-forbidden bands which overlap the more intense ligand-to-metal [$t_1(L) \rightarrow 3d$] charge transfer transitions. The spectra of the latter compound were found to be affected by the lower symmetry already at low Fe^{3+} concentrations (x = 0.01 (7)); aside from the fine structure due to this symmetry lowering, the experimental data are in support of the theoretical values in Table 5. It is seen from Fig. 8 and Table 5 that the $^6A_1$ ground state is shared almost equally between the d^5 and the d^6L configurations, while d^6L is the dominant contribution in the $^4T_1$, $^4T_2$, and $^2T_2$ excited states connected with the negative sign of the parameter Δ, which places d^6L at a lower energy than d^5. The larger contribution of d^5 to the ground state as compared to the lowest excited states is due to the gain of exchange energy, which is larger for the high-spin d^5 compared to the doublet and quartet states. As follows

TABLE 5

Transition Energies (cm^{-1}) and d^5 Percentage for the Ground and Lowest Excited States, Calculated Using a CI Charge Transfer Model for Tetrahedral FeS_4^{5-} [a]

State	$^6A_1$	$^4T_1$	$^4T_2$	$^2T_2$
Energy	0	7180	8630	12,560
% d^5	40	14	10	14

[a] Parameter values are Δ = −2.0 eV, 10Dq = 0.5 eV, T_1 = 1.4 eV, T_2 = 0.7 eV, U = 5 eV, and Q = 6 eV.

from Table 5 the transitions $^6A_1 \rightarrow {}^4T_1, {}^4T_2$, and $^2T_2$, which are normally viewed as "d–d" in a ligand field description, are in fact accompanied by a transfer of about 0.3 electrons from the metal to the ligand. This interpretation differs from the one proposed on the basis of spin-polarized $X\alpha$ calculations, attributing these transitions to a partial transfer of one electron in the opposite direction (25). In both interpretations, however, a single electron is strongly delocalized on the ligands and the orbital composition changes on excitation. The difference in the two interpretations may result from the distinctly smaller (compared to Ref. (25)) value of the parameter Δ indicated by our data. It was recently suggested (22) that ligand-field parametrization schemes such as the crystal field and the angular overlap models fail when the d^n and the $d^{n+1}L$ charge transfer configurations become strongly intermixed. In this regime, multiplets due to d^5 and d^6L couple to a different extent depending on their energy separation and hybridization. This prevents the use of a unique set of orbital and electron repulsion parameters as is usually done in ligand-field theory. Alternatively, any fitting procedure using such approaches may result in rather unrealistic parameter values [e.g., low values of B for FeS_4^{5-}, $B = 22$ cm^{-1}; see (25), B(free Fe^{3+}) = 1100 cm^{-1}]. For such systems all symmetry aspects are still at work, as nicely reflected by Fig. 8; however, the ligand-field approach per se loses its quantitative power. A similar effect was also shown in the spin-forbidden transitions of high-valent tetraoxo-coordinate tetrahedral Mn^{5+} and Fe^{6+} ions (30).

III.5. On the Spin-Ground States of d^5 Ions in Tetrahedral Coordination

The X-ray absorption data unambiguously show that the FeS_4^{5-} tetrahedra in both compounds Na_5FeS_4 and $KFeS_2$ are in a high-spin ground state. The intra-atomic exchange stabilization which favors the $S = 5/2$ state apparently dominates the ligand-field stabilization, which tends to lower the $S = 1/2$ and $S = 3/2$ states energetically. According to the Tanabe–Sugano diagrams for d^5 metals in cubic fields (31), intermediate spin states ($S = 3/2$) cannot become the lowest in energy. However, the situation may drastically change when negative Δ_{eff} values are allowed. In this case d^6L becomes lower in energy than d^5 and the $S = 3/2$ state may serve as alternative ground state of the FeS_4^{5-} cluster, ensuring high-spin local momenta ($S = 2$) for $Fe^{2+}(d^6)$, in accordance with the Hund's rule. An $S = 3/2$ ground state has been suggested from the interpretation of the Co2p XAS spectrum for the d^5 compound $SrCoO_3$ (32). In view of these results, it would be interesting to see how variations in 10Dq and Δ_{eff} affect the spin state of lowest energy for the FeS_4^{5-} cluster. For this purpose we performed calculations restricting to the lowest energy states of high-, intermediate-, and low-spin, $S = 5/2$, 3/2, and 1/2, respectively, for d^5 and the corresponding d^6L and d^7L^2 charge transfer states. A phase diagram indicating ranges of stability for the pure unmixed ground states ($T_t = T_e = 0$) as a function of the parameters 10Dq and Δ_{eff} is plotted in Fig. 9a. The chosen parameter values are the same as for the high-spin states (Table 2, $J = 0.863$ eV) with the only exceptions being 10Dq and Δ_{eff}, which were treated as variable parameters. A diagram analogous to Fig. 9a but accounting for mixing between the d^5, d^6L, and d^7L^2 multiplets due to hybridization using values of T_e and T_t from Table 2 (0.7 and 1.4 eV, respectively) is plotted in Fig. 9b. In the following, the d^7L^2 configuration will be neglected for reasons of simplicity; however, its effect on the calculations and the phase separation lines (Fig. 9b) was accounted for. A spin–orbit energy diagram representing all the necessary spin configurations for d^5, d^6L, their zero-order energies and mixing via hybridization is depicted in Fig. 10. In Fig. 10 we have shown the $^6A_1$ high-spin ($S = 5/2$), the $^4T_1$ intermediate-spin ($S = 3/2$), and the $^2T_2$ low-spin ($S = 1/2$) states of d^5 with their charge transfer states of t_2 and e symmetry. The other intermediate spin state, $^4T_2$, is found to be at about 1500 cm^{-1} higher energy than $^4T_1$ due to a less favorable Coulomb exchange (see above). The $^6A_1$ (d^5) state hybridizes with the ligand hole states of t_2 symmetry, which have an $e^2t_2^4$ configuration on metal. This state is 10Dq higher in energy compared to the normal high-spin $e^3t_2^3$ state resulting from the $d^6e(L)$ configuration. The low-spin $^2T_2$ (d^5) hybridizes with a $d^6t_2(L)$ state, which has the intermediate spin configuration $e^4t_2^2$. The intermediate spin $^4T_1$ (d^5) state hybridizes with a $d^6t_2(L)$ state, which has a high-spin $e^3t_2^3$ configuration on the metal. As follows from Fig. 10, both the high-spin $d^6e(L)$ and the intermediate-spin $d^6t_2(L)$ charge transfer states are favored by the crystal field, in contrast to the high-spin $d^6t_2(L)$, which is 10Dq higher in energy. Double-hole, charge transfer states yield a minor contribution to the ground state energy (as long as U_{eff} is much larger than Δ_{eff}) but they stabilize mainly the low-spin state. It should be noted that without hybridization the high-spin d^5 ($^6A_1$) and the d^6L ($^4T_1$) ground states are the only alternatives as long as 10Dq $< 3J$ and the low-spin d^5 ground state is not stabilized. In this case it is the high-spin state $^6A_1$ which is most stable when 10Dq is larger than Δ_{eff}; otherwise ($\Delta_{eff} <$ 10Dq) the intermediate-spin state becomes most stable as long as the t_2–e splitting of the ligand levels (δW) takes nonzero values. The latter increases the energy of the $d^6e(L)$ high-spin state with respect to the $d^6t_2(L)$ intermediate spin state (see Fig. 10). The $S = 5/2 \rightarrow S = 1/2$ spin crossover for the d^5 configuration, as predicted by the Tanabe–Sugano diagrams, may only occur when Δ_{eff} becomes sufficiently large ($\Delta_{eff} > 3J$); otherwise the $S = 5/2$ and $S = 1/2$ d^5 regions become separated by an intermediate $S = 3/2$ d^6L region. The mixing of d^5 states with d^6L states due to hybridization

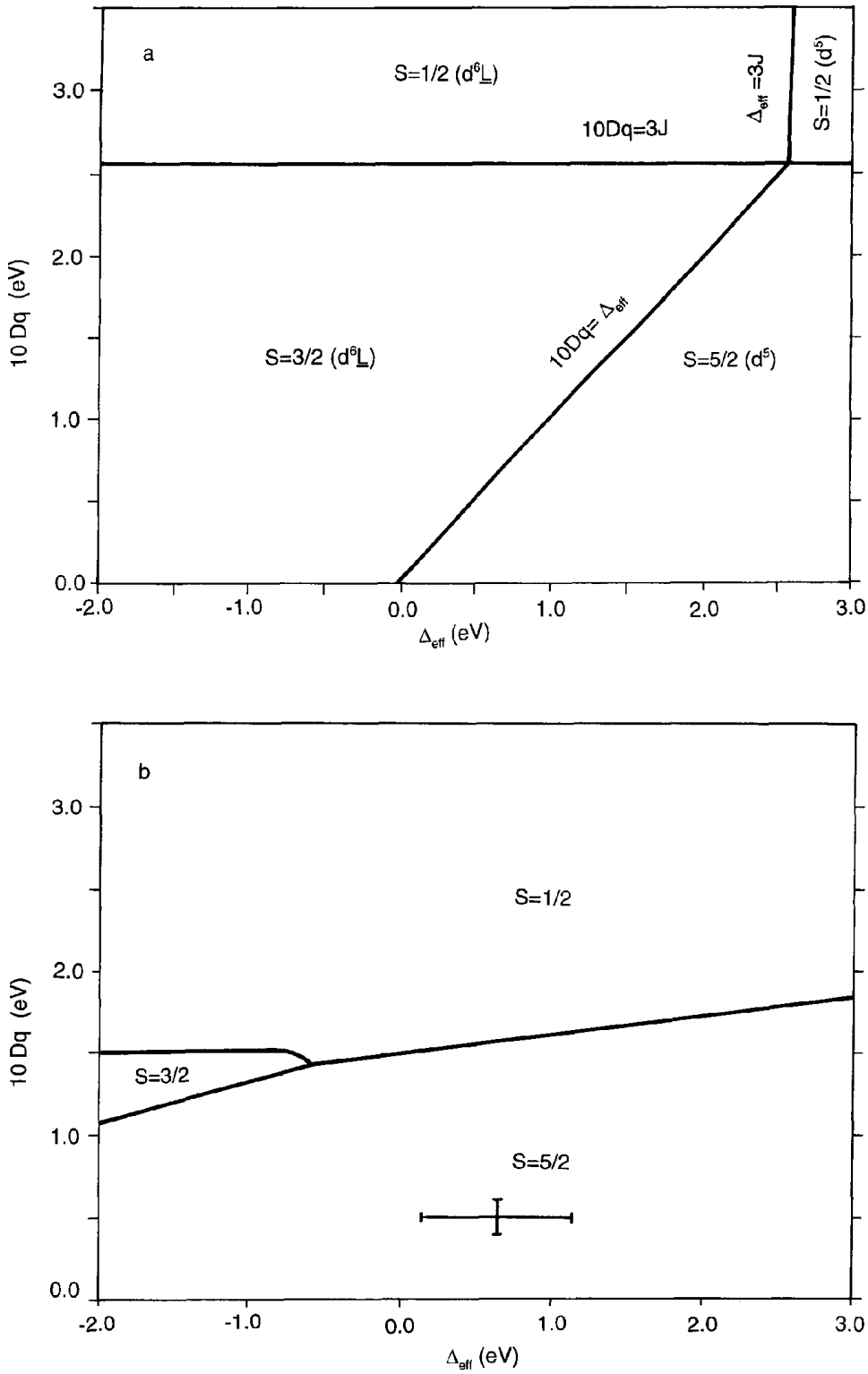

FIG. 9. Regions of stability for high- (S = 5/2), low- (S = 1/2), and intermediate-spin (S = 3/2) ground states in isolated FeS_4^{5-} tetrahedra without ($T_t = T_e = 0$) (a) and accounting for (T_t = 1.4 eV, T_e = 0.7 eV) (b) Fe(3d)–S(3s,3p) hybridization in dependence of the crystal field splitting parameter 10Dq and the effective charge transfer energy Δ_{eff}. The point approximately representing the ground state of FeS_4^{5-} in Na_5FeS_4 is also indicated. Values of J and U_{eff} are 0.863 and 10.37 eV, respectively (see text and Table 3).

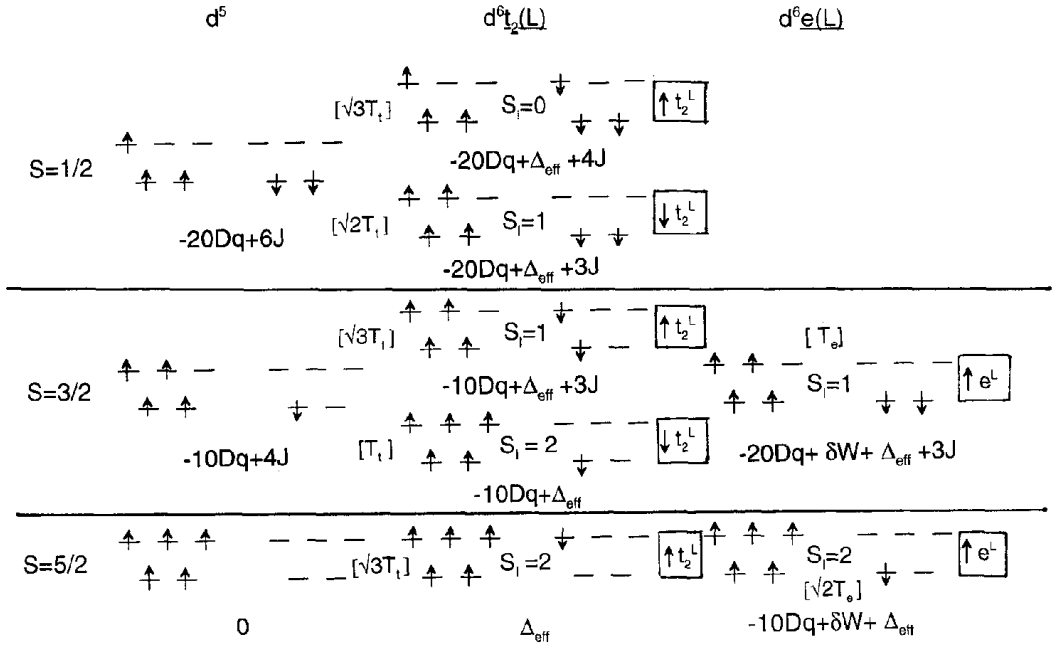

FIG. 10. Possible spin states for the ionic d^5 and their counterparts from the corresponding singly (d^6L) excited charge transfer configurations in tetrahedral symmetry.

(T_t nonzero) is most pronounced for the high-spin S = 5/2 ($\sqrt{3}T_t$), followed by the low-spin S = 1/2 ($\sqrt{2}T_t$) and intermediate S = 3/2 (T_t) spin states which can be seen in Fig. 10. Comparing Figs. 9a and 9b, the high-spin stability region is larger and has shifted toward the lower Δ_{eff} values due to the higher admixture of d^5 character in the ground state. The low-spin–high-spin separation lines are moved correspondingly toward lower 10Dq values, due to the increased exchange energy in the d^6L low-spin state (Fig. 10), which is of intermediate-spin character for d^6. For sufficiently low values of the parameter Δ_{eff}, the drop of the d^6L high-spin state due to covalency and exchange stabilization from mixing with d^5 is not enough to overcome the stabilization of the S = 3/2 (d^6L) state; as a result the intermediate spin-state region is achieved. The neglect of the splitting in the ligand levels δW leads to a narrowing of the intermediate state region, accompanied by a shift of the crossing point for the S = 5/2, 3/2, and 1/2 states toward lower values of Δ_{eff}. Thus for the parameter range adopted in Fig. 9b the intermediate spin range disappears when taking δW = 0.

In Fig. 9b we also indicated the point which, according to the parameter set in (Table 3, high-spin parameters), represents the high-spin state of FeS_4^{5-} in Na_5FeS_4. This point is energetically well separated from the S = 3/2 and S = 1/2 stability ranges (cf. Table 5), in contrast with the S = 3/2 ground state region where S = 1/2 and S = 5/2 excited states become quite close in energy. Therefore one hardly expects that ground states such as S = 3/2 or S = 1/2 for tetrahedrally coordinated Fe^{3+} may become stabilized, using chemical manipulations leading to dimers or higher oligomers.

IV. CONCLUDING REMARKS

1. Experimental L-edge X-ray absorption spectra of Na_5FeS_4 are well reproduced using atomic multiplet calculations in which covalency has been taken into account. The S = 5/2 ground state deduced from this interpretation is in good agreement with optical and magnetic susceptibility data (7, 14). The XAS spectra on $KFeS_2$ and a theoretical analysis strongly indicate that the FeS_4^{5-} tetrahedra are best described as being of high spin as well. Calculations of the ground state energies in dependence on the model parameters allow one to locate the FeS_4^{5-} ground state on a diagram with lines separating regions of stability for the possible S = 5/2, 3/2, and 1/2 ground states. The parameter values for FeS_4^{5-} in Na_5FeS_4 (Δ_{eff} = 0.68 eV, 10Dq = 0.5 eV, and T_t = 1.4 eV), deduced from a fit to the observed band profile, allow one to characterize the S = 5/2 ground state as energetically well separated from the S = 1/2 and S = 3/2 states. Therefore, solid-state effects such as low symmetric ligand fields, which manifest themselves when going from separate to interconnected FeS_4^{5-} units, can hardly change the ground state to low (S = 1/2) or intermediate (S = 3/2) ground states, in contrast to octahedrally coordinated Fe^{3+} ions. In the latter cases, low-spin–high-spin equilibria are frequently encountered and a first example of an S = 3/2 ground state (in $SrCoO_3$) with negative Δ have been also indicated (32). ESR data give further

support for the high-spin Fe^{3+}: the g value in $KFeS_2$ (g = 2.03 (33, 34)) is indeed very close to the spin-only value, showing (as expected for $S = 5/2$) negligible orbital contributions. A high-spin ground state for Fe^{5+} is also indicated by the vanishingly small magnetic anisotropies reported from inelastic neutron scattering experiments on $KFeS_2$ (34) and $TlFeS_2$ (35) and $X\alpha$ valence bond scattered wave calculations on $Fe(SR_4)^{1-}$ and $FeS_2(SR_4)^{2-}$ clusters (R = H, CH_3) (14). In view of the high-spin configuration on Fe^{3+} a reinterpretation of the magnetic susceptibility data and neutron scattering experiments based on $TlFeS_2$ (S = 3/2, (35)), Na_3FeS_3 (S = 3/2, (16)), and $KFeS_2$ (S = 1/2, (5, 15)) would be highly desirable. The unusually low-ordered moments seen in the neutron scattering and the very low magnetic hyperfine field from Mössbauer data (6) can be only partly explained by the small S to Fe charge transfer energy, which leads to an almost 1:1 admixture of d^5 and d^6L functions in the ground state already in the separate FeS_4^{5-} units. Another important contribution might result from the partial compensation of up and down spin densities as well as from important contributions of the 4s orbitals of iron.

The spin-densities on iron, [(3d) ↑ 4.94 (3d) ↓ 1.11 (4s) ↑ 0.43 (4s) ↓ 0.42], and the calculated hyperfine field of 250 kG (in good agreement with the magnitude of the experimental value 221 kG in $KFeS_2$ (6)) as deduced from $X\alpha$ calculations (13) are indeed quite compatible with a local high-spin state for Fe. In view of this, it should be noted that the rather low magnetic moments deduced from inelastic neutron scattering experiments may result from form-factor values considerably affected by covalency.

2. The main effects which result when going from FeS_4^{5-} to chains is the apparent lowering of symmetry around Fe^{3+} from almost T_d (separate FeS_4^{5-} units in Na_5FeS_4) to D_{2d} ($KFeS_2$). This is reflected by the strongly polarized absorption spectra (7) and quadrupolar splittings from Mössbauer data (6). Strong polarization effects due to S–S intrachain interactions are also indicated by some anisotropic Van Vleck susceptibilities in the chain compound $TlFeS_2$ (35). A calculation on an FeS_8^{16-} cluster which accounts for ligand–ligand overlap shows that the symmetry lowering around Fe^{3+} is accompanied by a shift of the d orbitals to higher energies, which is particularly pronounced for the MO orbital of $3d_{z2}$ type. This is drawn here as an explanation for the broadening of the XAS profile to higher energies from Na_5FeS_4 to $KFeS_2$. Dipolar magnetic fields due to the symmetry lowering may serve another contribution to the rather supressed magnetic moments reflected by the Mössbauer data.

3. The parameter values derived from the X-ray absorption data show a strong intermixing of multiplets originating from the d^5 and d^6L configurations. It is found that the $^6A_1$ and $^4T_1$, $^4T_2$, and $^2T_2$ originating from the d^5 configuration are involved in a different coupling to corresponding states of d^6L of the same spin and symmetry. The resulting bonding and/or Coulomb repulsion effects differ from one multiplet to another. For such systems ligand-field (crystal field or angular overlap model) interpretations of optical data (such as given in Ref. (7)) are found not to be applicable because they make use of sets of one- and two-electron quantities which are approximated as common for all d^5 multiplets.

ACKNOWLEDGMENTS

We are grateful to Prof. Dr. W. Bronger and Dr. P. Müller for the kind support of this work and the compounds investigated. Thanks are due to Dr. B. T. Thole for many helpful discussions. The receipt of an Alexander von Humboldt Fellowship (for 1992–1993) and a Volkswagen-Stiftung Fellowship (for 1994–1995) by one of us (M.A.) is gratefully acknowledged. This work was supported by the Netherlands Foundation for Fundamental Research on Matter (FOM), the Netherlands Foundation for Chemical Research (SON), the Netherlands Organization for the advancement of Pure Research (NWO), and the committee for the European Development of Science and Technology (CODEST) program.

REFERENCES

1. K. O. Klepp and W. Bronger, *Z. Anorg. Allg. Chem.* **532,** 23 (1986).
2. P. Müller and W. Bronger, *Z. Naturforsch. B.* **34,** 1264 (1979).
3. (a) W. Bronger, *Z. Anorg. Allg. Chem.* **359,** 225 (1968); (b) W. Bronger, *Angew. Chem. Int. Ed. Engl.* **20,** 52 (1981).
4. W. Bronger and P. Müller, *J. Less-Common Met.* **70,** 253 (1980).
5. W. Bronger, A. Kyas, and P. Müller, *J. Solid State Chem.* **70,** 262 (1987).
6. (a) H. P. Nissen and K. Nagorny, *J. Phys. Chem. NF* **95,** 301 (1975); (b) H. P. Nissen and K. Nagorny, *Z. Phys. Chem. NF* **99,** 209 (1976).
7. R. Packroff and H.-H. Schmidtke, *Inorg. Chem.* **32,** 654 (1993).
8. C. A. Taft and M. A. de Paoli, *Chem. Phys. Lett.* **68,** 94 (1979).
9. J. Silvestre and R. Hoffmann, *Inorg. Chem.* **24,** 4108 (1985).
10. H.-H. Schmidtke, U. Rosellen, and M. Diel, *Mol. Phys.* **83,** 1191 (1994).
11. J. G. Norman, B. J. Kalbacher, and S. C. Jackels, *Chem. Commun.,* 1027 (1978).
12. J. G. Norman, P. B. Ryan, and L. Noodleman, *J. Am. Chem. Soc.* **102,** 4279 (1980).
13. (a) C. A. Taft and M. Braga, *Phys. Rev. B* **21,** 5802 (1980); (b) S. K. Lie and C. A. Taft, *Phys. Rev. B* **28,** 7308 (1983).
14. L. Noodleman, J. G. Norman, Jr., J. H. Osborne, A. Aizman, and D. A. Case, *J. Am. Chem. Soc.* **107,** 3418 (1985).
15. W. Bronger and P. Müller, *J. Less-Common Met.* **100,** 241 (1984).
16. W. Bronger, U. Ruschewitz, and P. Müller, *J. Alloys Compounds* **176,** 167 (1991).
17. W. A. Harrison, "Electronic Structure and the Properties of Solids—The Physics of the Chemical Bond." Freeman, San Francisco, 1980.
18. P. H. Butler, "Point Group Symmetry, Applications, Methods and Tables." Plenum, New York, 1981.
19. (a) R. D. Cowan, *J. Opt. Soc. Am.* **58,** 808 (1968); (b) R. D. Cowan, "The Theory of Atomic Structure and Spectra." Univ. of California Press, Berkeley, 1981.
20. (a) B. T. Thole, unpublished results; (b) G. van der Laan, B. T. Thole, G. A. Sawatzky, and M. Verdaguer, *Phys. Rev. B.* **37,** 6587 (1988); (c) G. van der Laan and I. W. Kirkman, *J. Phys. Condens. Matter* **4,** 4189 (1992) and references cited therein; (d) F. M. F. de Groot,

J. C. Fuggle, B. T. Thole, and G. A. Sawatzky, *Phys. Rev. B* **42,** 5459 (1990).
21. J. C. Slater and G. F. Koster, *Phys. Rev.* **94,** 1498 (1954).
22. G. A. Sawatzky, "On the Electronic Structure and Related Physical Properties of 3*d* Transition Metal Compounds," Proceedings, Spring College in Condensed Matter on Superconductivity, Trieste, 1992.
23. (a) A. E. Bocquet, T. Saitoh, T. Mizokawa, and A. Fujimori, *Solid State Commun.* **83,** 11 (1992); (b) A. E. Bocquet, T. Mizokawa, T. Saitoh, H. Namatame, and A. Fujimori, *Phys. Rev. B* **46,** 3771 (1992).
24. M. Fujisawa, S. Suga, T. Mizokawa, A. Fujimori, and K. Sato, *Phys. Rev. B* **49,** 7155 (1994).
25. K. D. Butcher, M. S. Gebhard, and E. I. Solomon, *Inorg. Chem.* **29,** 2067 (1990).
26. D. Alders, J. Vogel, C. Levelut, S. D. Peacor, M. Sacchi, G. van der Laan, B. T. Thole, and G. A. Sawatzky, to be published.
27. (a) M. van Veenendaal, D. Alders, and G. A. Sawatzky, unpublished results; (b) M. van Veenendaal, "The Theory of Core-Level Line Shapes beyond the Impurity Model." Thesis, University of Groningen, 1994.
28. G. A. Sawatzky and J. Hupkes, *Phys. Rev. Lett.* **25,** 100 (1970).
29. J. C. Deaton, M. S. Gebhard, S. A. Koch, M. Millar, and E. I. Solomon, *J. Am. Chem. Soc.* **110,** 6241 (1988).
30. M. Atanasov, *Chem. Phys.* **195,** 49 (1995).
31. S. Sugano, Y. Tanabe, and H. Kamimura, "Multiplets of Transition Metal Ions in Crystals." Academic Press, New York, 1970.
32. R. H. Potze, G. A. Sawatzky, and M. Abbate, submitted for publication.
33. W. V. Sweeney and R. E. Coffman, *Biochim. Biophys. Acta* **286,** 26 (1972).
34. M. Nishi, Y. Ito, and S. Funahashi, *J. Phys. Soc. Jpn.* **52,** 2210 (1983).
35. D. Welz and M. Nishi, *Phys. Rev. B* **45,** 9806 (1992).